JOURNAL OF GEOPHYSICAL RESEARCH, VOL. 113, C06011, doi:10.1029/2007JC004596, 2008

Limiting states of internal wave rays

Fan Ping[1] and V. P. Singh[2]

Received 19 October 2007; revised 22 January 2008; accepted 28 February 2008; published 13 June 2008.

[1] Existing models of baroclinic tides are based upon the "traditional approximation", i.e., neglect of the horizontal component of the Earth's rotation, leading to a well-known conclusion that no freely propagating internal waves can exist beyond the critical latitude and the wave rays are symmetric to the vertical. However, recent studies have contended that the situation may change if both the vertical and horizontal components of the Earth's rotation are taken into account. With the full account of the Coriolis force, characteristics of the internal wavefield generated by tidal flow over uneven topography are investigated. It is found that "nontraditional effects" profoundly change not only the dynamics of internal waves but also the rate at which the barotropic tidal energy is fed into the internal wavefield. Discarding the traditional approximation, internal waves are proved to be able to generate poleward of the critical latitude, rays of which are no longer symmetric and the limiting values of ray angles become greater or less than 90°, depending on the local latitude and the direction of ray. More importantly, in contrast to the predictions of models based upon the traditional approximation, a substantial conversion occurs in the situations when stratification is so weak that the buoyancy frequency is below the tidal one.

Citation: Fan, P., and V. P. Singh (2008), Limiting states of internal wave rays, *J. Geophys. Res.*, *113*, C06011, doi:10.1029/2007JC004596.

1. Introduction

[2] It has long been known that existing linear models of baroclinic tides enable us to easily examine the impact of different external parameters on the internal tide generation [*Garrett and Kunze*, 2007]. However, consideration of baroclinic tides under the traditional approximation encounters a serious difficulty that a latitude θ exists, where the tidal frequency ω_0 equals the inertial frequency, which coincides with the value of the Coriolis parameter f ($f = 2\Omega \sin\theta$, $\Omega = 7.292 \times 10^{-5}$ s^{-1} is the frequency of the Earth's rotation), beyond which no real linear solution exists. In other words, the existence of periodic baroclinic tides above the critical latitude is prohibited. This contrasts significantly with the evidence of semidiurnal internal tides above the critical latitude revealed recently by the experimental data of *Pisarev* [1996], *Parsons et al.* [1996], and *Vlasenko et al.* [2003]. A likely explanation that lies in the inclusion of the nontraditional term (the horizontal component of the Earth's rotation) was first presented by *Gerkema and Shrira* [2005a]. They remarked that internal tides could exist up to several degrees beyond the critical latitude if nontraditional effects were taken into consideration. However, further calculations are still required to support their argument.

[3] Nontraditional effects are currently receiving renewed attention due to their unique role in ocean dynamics. An early insight into the nontraditional effects is nowadays accepted, that is, consideration of nontraditional terms can enlarge the frequency range for internal waves [*Saint-Guily*, 1970; *LeBlond and Mysak*, 1978; *Miropol'sky*, 2001; *Gerkema and Shrira*, 2005b, and the references therein]. Apart from this fundamental understanding, effects of nontraditional terms have been discussed in some detail in recent years. On the basis of some preliminary calculations *Baines and Miles* [2000] argued that the inclusion of "nontraditional" terms can produce a change of the propagation direction of the internal wave energy. Furthermore, the combined effects of the nontraditional terms and β effect are elucidated by *Gerkema and Shrira* [2005a]. In their most significant contribution, *Gerkema and Shrira* [2005b] first provided a comprehensive discussion of the vertical structures of internal waves and found that nontraditional effects significantly altered not only the wave propagation but also the conditions for critical reflection for near inertial internal waves. Besides these theoretical works, a number of important field experiments have been carried out by *Van Haren and Millot* [2004, 2005] and *Van Haren* [2006], who provided substantial evidence for the existence of nontraditional effects from observations in the Mediterranean Sea and Irminger Sea.

[4] Thus attributes of the internal tides created by nontraditional effects are becoming of special oceanographic interest and deserve an in-depth and quantitative discussion. Given this interest in oceanography, a primary and specific objective of this paper is to clarify the role of nontraditional terms in dissimilar gradients of internal beams and their

[1]Institute of Mechanics, Chinese Academy of Sciences, Beijing, China.
[2]Department of Biological and Agricultural Engineering, Texas A & M University, College Station, Texas, USA.

0148-0227/08/2007JC004596$09.00

unique role in tidal conversion. This may help enhance our fundamental understanding of the dynamics of internal tides. The paper is organized as follows. In section 2, the problem of internal wave generation is formulated by taking the horizontal component of the Earth's rotation into consideration. General solutions of internal waves produced by tidal flow over topographies are derived in section 3, and properties of the solutions are discussed. In section 4 the tidal conversion caused by a Gaussian topography is calculated and compared with the results under the traditional approximation. Section 5 concludes the paper.

2. Formulation

[5] The linearized equations governing the motion of a density-stratified Boussinesq fluid of ambient density $\rho_0(z)$ on the f-plane with full account of the Coriolis force can be expressed as:

$$\begin{aligned} u_t - fv + f_h w &= -\frac{1}{\rho_0}p_x, \qquad v_t + fu = -\frac{1}{\rho_0}p_y, \\ w_t - f_h u &= -\frac{1}{\rho_0}p_z - \frac{\rho}{\rho_0}g, \qquad u_x + v_y + w_z = 0, \\ \rho_t &= \frac{\rho_0}{g}N^2 w \end{aligned} \tag{1}$$

in which N denotes the constant buoyancy frequency; ρ is the perturbed density; p is the pressure; g is the gravitational acceleration; x (west-east), y (south-north) and z (vertical, positive upward with the origin at the undisturbed surface) are the Cartesian coordinates; u, v, w are the corresponding velocity components; the Coriolis vector can be represented as $(0, f_h, f) = 2\Omega = 2\Omega\ (0, \cos\theta, \sin\theta)$, in which Ω is the angular velocity of the earth; and θ is the latitude.

[6] In the traditional approximation, one would take $f_h = 0$ [*Eckart*, 1960]. Here, one-dimensional topography $z = -H(y)$ is considered, and hence $\partial/\partial x \equiv 0$. Thus the model equation and linearized boundary conditions in the y-z plane containing only $w(y, z, t)$ take the form (initially at rest):

$$\begin{aligned} &\left(\partial_{tt} + f^2\right)w_{zz} + 2ff_h w_{yz} + \left(N^2 + \partial_{tt} + f_h^2\right)w_{yy} = 0, \\ &w(y,0,t) = 0, \quad w(y,-h_0,t) = UH_y = \mathrm{Re}\left[U_0 H_y e^{i\omega_0 t}\right] \end{aligned} \tag{2}$$

where $U = U_0\cos\omega_0 t$ is the velocity of the background flow. Applying the Laplace transform with respect to t and the Fourier transform with respect to y to equation (2) one gets the following boundary value problem:

$$\begin{aligned} &\left(s^2 + f^2\right)\tilde{\bar{w}}_{zz} + 2iff_h k\tilde{\bar{w}}_z - \left(N^2 + s^2 + f_h^2\right)k^2\tilde{\bar{w}} = 0 \\ &\tilde{\bar{w}}(k,0,s) = 0, \quad \tilde{\bar{w}}(k,-h_0,s) = U_0\frac{ik\overline{H}(k)}{s - i\omega_0} \end{aligned} \tag{3}$$

Furthermore, the transformation

$$\tilde{\bar{w}}(k,z,s) = \varphi(k,z,s)e^{-\frac{iff_h kz}{s^2+f^2}} \tag{4}$$

leads to the following boundary value problem for φ:

$$\varphi_{zz} + K^2\varphi = 0 \varphi(0) = 0, \quad \varphi(-h_0) = \tilde{\bar{w}}(-h_0)e^{\frac{-iff_h k}{s^2+f^2}h_0} \tag{5}$$

where

$$K^2 = -\frac{(N^2 + s^2)(s^2 + f^2) + s^2 f_h^2}{\left(s^2 + f^2\right)^2}k^2 = \mu^2(s)k^2 \tag{6}$$

Obviously, μ^{-1} denotes the slope of internal gravity wave rays generated by the tide on the nontraditional f-plane. Returning to the solution of the problem, one can readily identify that the zero points of function $\mu(s)$ are $s = \pm i\omega_{1,2}$, $(\omega_1 > \omega_2)$, satisfying:

$$\omega_{1,2}^2 = \frac{N^2 + f^2 + f_h^2}{2}\left[1 \pm \sqrt{1 - \frac{4N^2 f^2}{\left(N^2 + f^2 + f_h^2\right)^2}}\right] \tag{7}$$

It is easy to check that $\omega_1^2 > N^2$ and $\omega_2^2 < f^2$. This indicates that the frequency range of the free propagating internal waves is enlarged due to the inclusion of the nontraditional term f_h, which is in agreement with *LeBlond and Mysak* [1978] and *Gerkema and Shrira* [2005b].

[7] The general solution of equation (5) can be expressed as

$$\varphi(z) = -U_0\frac{\sin Kz}{\sin Kh_0}\frac{ik\overline{H}(k)}{s - i\omega_0}e^{\frac{-iff_h k}{s^2+f^2}h_0} \tag{8}$$

Substituting equation (8) into equation (4) and applying the inverse Laplace and Fourier transforms yield the solution of equation (2) as:

$$w(z) = -\frac{U_0}{\sqrt{2\pi}}\int_{-\infty}^{\infty}\frac{ik\overline{H}(k)}{2\pi i}\int_{Br}\frac{\sin Kz}{\sin Kh_0}\frac{e^{ik\xi(y,s)}e^{st}}{s - i\omega_0}dsdk \tag{9}$$

where $\xi(y, s) = y - ff_h(z + h_0)/(s^2 + f^2)$. For $K > 0$, the poles of the integrand in equation (9) are $s = i\omega_0$, $\pm i\omega_{1m}(k)$, and $\pm i\omega_{2m}(k)$, the latter two of which satisfy $\mu^2(\pm i\omega_{1m}) = \mu^2(\pm i\omega_{2m}) = (m\pi/kh_0)^2$, $(\omega_{1m} > f > \omega_{2m} > 0,\ m = 1, 2, \ldots)$. With the application of the residue theorem, the integrals involved in equation (9) can be evaluated and hence simplified into (for superinertial waves, $\omega_0 > f$),

$$w(\xi_1,z,t) = \begin{cases} \sqrt{2\pi}\dfrac{U_0}{h_0}\displaystyle\sum_{m=1}^{\infty}(-1)^m\frac{k_m}{\mu_0}\overline{H}(k_m)\sin\frac{m\pi z}{h_0}\cos(k_m\xi_1 - \omega_0 t), & \xi_1 > 0 \\ \sqrt{2\pi}\dfrac{U_0}{h_0}\displaystyle\sum_{m=1}^{\infty}(-1)^{m+1}\frac{k_m}{\mu_0}\overline{H}(k_m)\sin\frac{m\pi z}{h_0}\cos(k_m\xi_1 + \omega_0 t), & \xi_1 < 0 \end{cases} \tag{10}$$

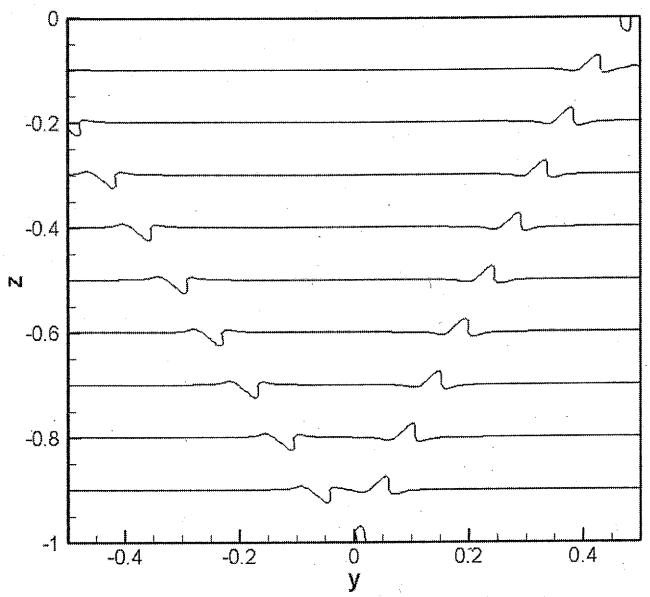

Figure 1. Snapshot of the buoyancy field computed from equation (10) for a Gaussian topography profile. Parameters are $\omega_0 = 1.405 \times 10^{-4}$ s^{-1}, $N^* = 10$, $h_0 = 5000$ m, $H_0 = 0.1$ h_0, $\gamma = 1$, $U_0 = 0.01$ ms^{-1}, $m = 100$, $t = 12$ h, and $\theta = 70°$. The maximal elevation of isotherms is found to be 3.67 m. To make the radiating internal tide visible, the horizontal coordinate y, the vertical coordinate z, and the wave amplitude are normalized, respectively, by the total horizontal length $Y = 200$ km, the total depth h_0 and $h_0/50$.

For the subinertial case, the vertical velocity becomes:

$$w(\xi_1,z,t) = \begin{cases} \sqrt{2\pi}\dfrac{U_0}{h_0}\displaystyle\sum_{m=1}^{\infty}(-1)^m\frac{k_m}{\mu_0}\overline{H}(k_m)\sin\frac{m\pi z}{h_0}\cos(k_m\xi_1+\omega_0 t), & \xi_1 > 0 \\ \sqrt{2\pi}\dfrac{U_0}{h_0}\displaystyle\sum_{m=1}^{\infty}(-1)^{m+1}\frac{k_m}{\mu_0}\overline{H}(k_m)\sin\frac{m\pi z}{h_0}\cos(k_m\xi_1-\omega_0 t), & \xi_1 < 0 \end{cases} \tag{11}$$

where $\mu_0 = \mu(i\omega_0)$, $k_m = m\pi/\mu_0 h_0$ ($m = 1, 2, \ldots$), and $\xi_1 = y + ff_h(z + h_0)/(\omega_0^2 - f^2)$.

[8] To visualize the solution, a topography whose shape has a Gaussian form $H(y) = H_0\exp(-y^2/2L^2)$ is chosen. Here, L parameterizes the horizontal scale of the topography. Figure 1 presents the buoyancy field computed from equation (10) for a Gaussian topography profile at a superinertial latitude $\theta = 70°$. It is evident that the internal wave rays originate from the topography and propagate poleward and equatorward with different angles. This is utterly different from the traditional understanding for internal waves. The maximal elevation of the isotherms ζ_m is found to be 3.67 m and hence the amplitude of the vertical velocity ($w_m = \omega_0\zeta_m$) is accordingly 5.16×10^{-4} ms^{-1}. Furthermore, from the continuity equation, one can easily find that the relationship between the amplitudes of the meridional and vertical velocities satisfy $v_m = w_m/|R_{\min}|$ (notice that $\partial/\partial x = 0$ and $|R_{\min}|$ denotes the minimum of the ray slopes), which leads to $v_m = 2.73 \times 10^{-2}$ ms^{-1}. Similarly, one can also identify from the first equation of equation (1) that the maximal zonal velocity satisfies $u_m = (fv_m - f_h w_m)/\omega_0 = 2.64 \times 10^{-2}$ ms^{-1}.

[9] On the other hand, in processes of equation (9), one may find the other part of the solution which comes from the poles $s = \pm i\omega_{1m}(k)$ if $\omega_0 > f$,

$$w'(z) = \frac{U_0}{\sqrt{2\pi}h_0}\sum_{m=1}^{\infty}(-1)^{m+1}\int_{-\infty}^{\infty} ik\overline{H}(k)\sin\frac{m\pi z}{h_0} \times\left[\frac{e^{ik\xi(i\omega_{1m})}e^{i\omega_{1m}t}}{(i\omega_{1m}-i\omega_0)K_s|_{s=i\omega_{1m}}}+\frac{e^{ik\xi(i\omega_{1m})}e^{-i\omega_{1m}t}}{(-i\omega_{1m}-i\omega_0)K_s|_{s=-i\omega_{1m}}}\right]dk \tag{12}$$

where the differentiation of K with respect to s can be evaluated from equation (6),

$$K_s = s\frac{(N^2-f^2)(s^2+f^2)+f_1^2(s^2-f^2)}{(s^2+f^2)^3K}k^2 \tag{13}$$

and the superinertial poles $\omega_{1m}(k)$ can be obtained from the relation $\mu^2(i\omega_{1m}) = (m\pi/kh_0)^2$ ± $m = 1, 2, \ldots$),

$$\omega_{1m}^2(k) = \frac{1}{2}\frac{N^2-f^2+f_1^2}{1+\left(\frac{m\pi}{kh_0}\right)^2} \cdot\left\{1+\sqrt{1+\frac{4f^2f_1^2\left[1+(m\pi/kh_0)^2\right]}{\left(N^2-f^2+f_1^2\right)^2}}\right\}+f^2 \tag{14}$$

The integrand involved in equation (12) takes on an asymptotic form as t becomes large, which is determined entirely in terms of where the phase $\psi(k) = k\xi(i\omega_{1m}) \pm \omega_{1m}t$ is stationary, that is, $d\psi/dk = 0$. Therefore the stationary points, $\pm k_p$, of the integral should satisfy the following relation:

$$\pm\frac{d\omega_{1m}}{dk} = \frac{\xi(i\omega_{1m})}{t}+\frac{k}{t}\frac{d}{dk}\xi(i\omega_{1m}) \tag{15}$$

With the application of the stationary phase method (see for instance, *Nayfeh* [1973] and *Lighthill* [1978]), the transient part of w' from the stationary points k_p for large t can be given by

$$w'(z) = \frac{U_0}{h_0}\sum_{m=1}^{\infty}(-1)^{m+1}\frac{k_p}{\sqrt{|\psi''(k_p)|}}\frac{\overline{H}(k_p)}{K_s(i\varpi_m,k_p)}\sin\frac{m\pi z}{h_0} \times\left[\frac{e^{i\left(k_p\xi_m+\varpi_m t+\frac{\pi}{4}\mathrm{sgn}\psi''(k_p)\right)}}{\varpi_m-\omega_0}+\frac{e^{i\left(k_p\xi_m-\varpi_m t+\frac{\pi}{4}\mathrm{sgn}\psi''(k_p)\right)}}{\varpi_m+\omega_0}\right] \tag{16}$$

where $\varpi_m = \omega_{1m}(k_p)$, $\xi_m = \xi(i\varpi_m)$, and $H(y)$ is assumed to be an even function. It is evident from the above equation that the remarkable feature of the transient part of the solution is of order $t^{-1/2}$, which makes the amplitude tend to zero as $t \to \infty$. As a result, in a long time period the steady part of the solution which can propagate a large distance with a permanent form is of more physical interest than the transient part.

3. Limiting States of the Internal Beams

[10] As mentioned in the introduction, although the role of nontraditional terms has been of increasing research interest in recent years, some more dynamics of internal waves, including the limiting states of the internal beams and the tidal conversion in full account of the Coriolis force, is still poorly understood. There is therefore a strong justification to more closely investigate the special properties of internal waves caused due to nontraditional effects.

[11] It is apparent from equations (10) and (11) that along the lines $K_m z = \pm k_m \xi_1$, (where $K_m = m\pi/h_0$) the wave phase keeps constant. These lines are readily identified as the characteristics of internal waves of frequency ω_0 or the internal wave rays. In keeping with the standpoint of the stationary phase [*Lighthill*, 1978], the wave energy is propagating nowhere but almost concentrating on these characteristic lines where the wave phase is stationary, which is shown apparently in Figure 1. Outside this range, the wave oscillations get evanescent rapidly. One remarkable property of internal tides is that the rays emitted from the topography make a fixed angle with the horizontal. Under the traditional approximation, the ray slopes are known as:

$$R_{1,2} = \pm\sqrt{\frac{\omega_0^2 - f^2}{N^2 - \omega_0^2}} \tag{17}$$

However, the presence of the horizontal component of Earth's rotation modifies the ray slopes to:

$$R_1 = \left(\mu_0 - \frac{ff_h}{\omega_0^2 - f^2}\right)^{-1}, \quad R_2 = -\left(\mu_0 + \frac{ff_h}{\omega_0^2 - f^2}\right)^{-1} \tag{18}$$

An impression one can have from equations (17) and (18) is that ray slopes differ fundamentally from those under the traditional approximation due to the inclusion of f_h, as confirmed by *Gerkema and Shrira* [2005b].

[12] To facilitate diagnosing the influence of external parameters, it is instructive to introduce the following dimensionless buoyancy and rotation frequencies based upon the timescale of the tide, i.e., $N^* = N/\omega_0$, $\Omega^* = 2\Omega/\omega_0$. As the frequencies of Earth's rotation $\Omega = 7.292 \times 10^{-5}$ s^{-1}, the nondimensional rotation frequency Ω^* is approximately equal to 1.038, and the critical value of the latitude satisfying $\theta_c = \sin^{-1}(1/\Omega^*)$ equals 74.5° for M_2 tide which has a frequency 1.405×10^{-4} s^{-1}. It is also noted that for internal tides of diurnal frequency (e.g., K_1, O_1 etc.) Ω^* is equal to 2 and θ_c becomes approximately 30°. Specifically, the frequency of the semidiurnal M_2 tide is taken as the characteristic timescale of discussion in the ensuing part.

With these dimensionless variables in hand, the ray slopes can be rewritten as:

$$R_1 = \left(\sqrt{\frac{(N^{*2}-1)(1-\Omega^{*2}\sin^2\theta) + \Omega^{*2}\cos^2\theta}{(1-\Omega^{*2}\sin^2\theta)^2}} - \frac{1}{2}\frac{\Omega^{*2}\sin 2\theta}{1-\Omega^{*2}\sin^2\theta}\right)^{-1},$$

$$R_2 = -\left(\sqrt{\frac{(N^{*2}-1)(1-\Omega^{*2}\sin^2\theta) + \Omega^{*2}\cos^2\theta}{(1-\Omega^{*2}\sin^2\theta)^2}} + \frac{1}{2}\frac{\Omega^{*2}\sin 2\theta}{1-\Omega^{*2}\sin^2\theta}\right)^{-1} \tag{19}$$

Given the above two meaningful equations, we will show below the unique behavior of the ray angles created by nontraditional effects, which significantly alter the traditional understanding of the dynamics of internal waves.

[13] Comparisons of the ray angles ν between with and without the traditional approximation are graphed in Figure 2, in which the lines (except the dash-dot lines denoting the limits of the ray angle and frequency) correspond to the right branches of rays and the scattered symbols to the left branches. Foremost, it is obvious from Figure 2a that angles of the right branches of rays are mirror-images (with respect to the horizontal line in this figure, $\nu = 90°$) of the left branches. By contrast, Figures 2b and 2c show asymmetry in the ray angles created by nontraditional effects, which accords well with the findings of *Durran and Bretherton* [2004] and *Gerkema and Shrira* [2005b].

[14] Furthermore, $\nu = 90°$ acts as the limiting value of ray angles for both the right branch and the left branch regardless of the nontraditional effect. This is understood from equation (17), because the denominator vanishes as $N^* \to 1$, while the numerator does not. The traditional approximation thus has the characteristic of a singular limit at $N^* = 1$, which is absent if the term f_h is considered. As is evident from Figures 2b and 2c, the singularity at $N^* = 1$ mentioned previously is removed by the nontraditional effects: for superinertial waves, angles of the right branches can exceed $\nu = 90°$ if N^* less than 1, while those of the left branches are always greater than 90°; for subinertial waves, the vice versa is true.

[15] To have a better understanding of how nontraditional effects affect the ray slopes of the internal waves, five typical examples of internal wave rays are presented in Figure 3, where the latitude θ and nondimensional buoyancy frequency N^* are: (1) 74°, 0.2; (2) 74°, 0.958; (3) 74°, 5; (4) 75°, 0.963; and (5) 75°, 3.3, respectively. The results for the maximal elevations of isotherms (ζ_m) and amplitudes of the velocity components (u_m, v_m, w_m) for each case are given in Table 1, where the formulae for calculating each of the velocity components are similar as mentioned previously for Figure 1.

[16] As is clear from Figure 3a, both of the equatorward rays are seen for superinertial wave with nondimensional frequency N^* less than 1. In Figures 3b and 3c, where the latitudes are the same as those in Figure 3a, increasing the buoyancy frequency changes the propagation of the right branch of the rays from equatorward to poleward, while the left branch remains in the equatorward direction. This is

understandable from the superinertial case illustrated in Figure 2b. In Figure 3e where the internal wave is subinertial and the dimensionless frequency N^* is greater than 1, the two branches appear to be both poleward. Obviously, these results show striking differences to the traditional understanding on the ray angles, and have been recognized by *Durran and Bretherton* [2004] and *Gerkema and Shrira* [2005b]. On the basis of these fundamental understandings on the nontraditional effects, one of the major aims of this study is to quantitatively examine the limiting values of the ray angles by abandoning the traditional approximation.

[17] In accord with the traditional approximation, the ray angle ν equal to 90° means that the internal wave propagates vertically and has no effect in the horizontal direction. The corresponding singular limit for the dimensionless buoyancy frequency $N_c^* = 1$. However, if the nontraditional effect is considered, the internal wave at such a value for N^* can still propagate to the horizontal due to the asymmetry attributes (seen from Figures 3b and 3d). The critical value of N^* where $\nu = 90°$ in this situation can be easily derived from equation (18) as:

$$N_c^{*2} = 1 - \Omega^{*2} \sin^2 \theta \tag{20}$$

For a given latitude less than the critical value ($\theta < \theta_c$), $N^* < N_c^*$ means that the ray angles are greater than 90°, while $N^* > N_c^*$ means that one of the rays is equatorward and the other propagates poleward. On the contrary, for a supercritical latitude, $N^* < N_c^*$ corresponds to the case that the rays propagate both equatorward and poleward, while, $N^* > N_c^*$ means that the ray angles are less than 90°.

[18] Figure 4 shows the dependence of N_c^{*2} on latitude θ. First, it is seen that the line denoting N_c^{*2} lies in the range of (0, 1), and is divided into two parts by the line $\theta = \theta_c$ (or $N_c^{*2} = 2 - \Omega^{*2}$). The part below the critical latitude θ_c represents the limiting value for the right branch and that above θ_c denotes the limiting value for the left branch. Apparently, the critical value of N^* has a maximum, 1, and that does not exist any longer for θ less than a minimum value, $\theta_m = \cos^{-1} \Omega^{*-1} \approx 15.55°$. This implies that below θ_m the internal waves can never propagate vertically, neither for those with frequency N larger than ω_0.

[19] On the other hand, another singular limit can be produced as well by the nontraditional effects at the critical latitude. We can find from equation (19) that as $\theta \to \theta_c$, R_1 tends to infinite, while R_2 drops to zero, equivalent to the case of the vertical propagating right branch and horizontal propagating left branch. Note that the nature of this singular limit at $\theta = \theta_c$ can be entirely changed by the traditional approximation, as implied by equation (17).

[20] It is also clear from equation (19) that the ray slopes R lie in a monotonic dependence on the dimensionless frequency N^*. As a result, the ray angles will reach their limit when $N^* = 0$ (in this limit the internal waves are pure gyroscopic and their existence has been revealed by *Van*

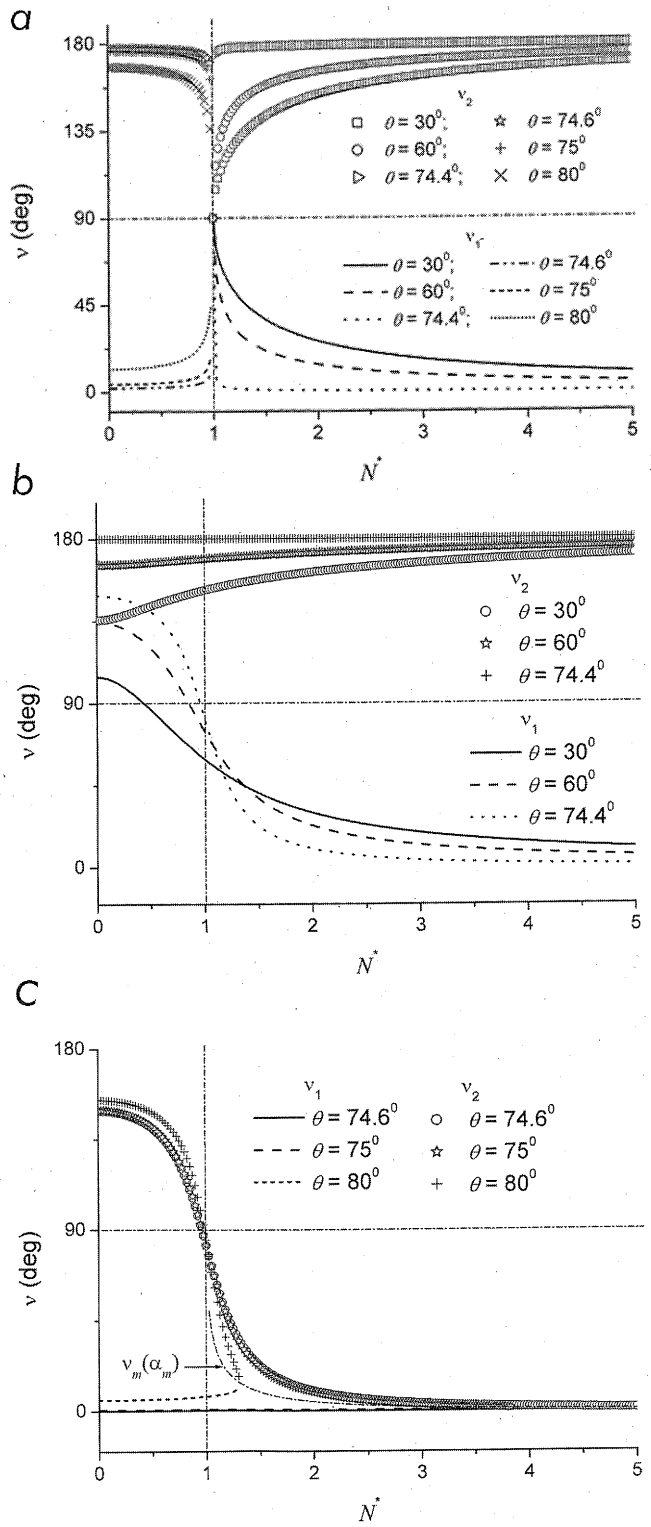

Figure 2. (a) Behavior of ray angles as functions of N^* for various values of θ [ray angles under the traditional approximation, lines correspond to the right branches of rays and scattered symbols to the left branches.]. (b) Behavior of ray angles as functions of N^* for various values of θ [ray angles of the superinertial frequencies ($\omega_0 > f$, or, $\theta < \theta_c$) with the inclusion of f_h, lines correspond to the right branches of rays and scattered symbols to the left branches]. (c) Behavior of ray angles as functions of N^* for various values of θ [ray angles of subinertial frequencies ($\theta > \theta_c$) with the inclusion of f_h, lines correspond to the right branches of rays and scattered symbols to the left branches].

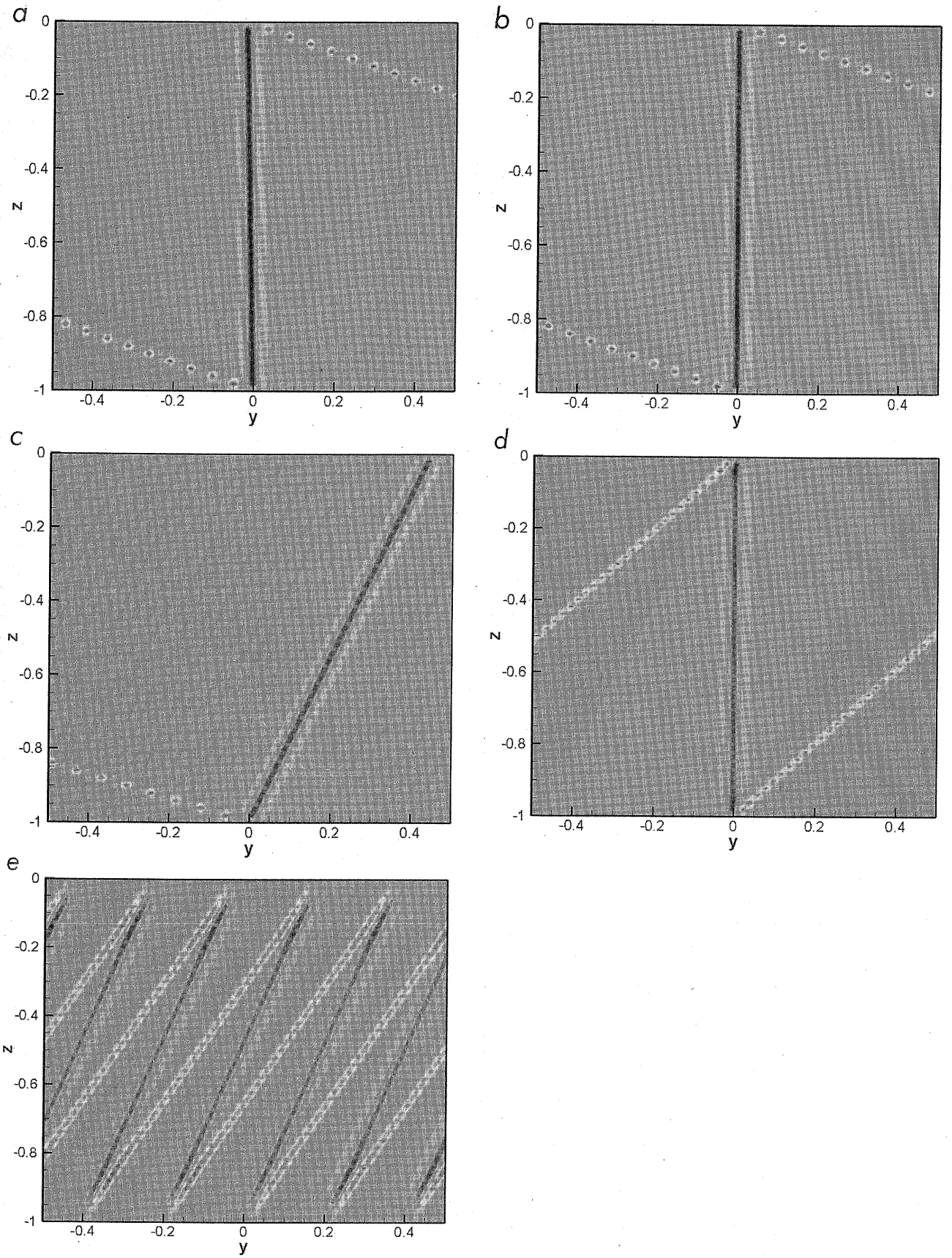

Figure 3

Table 1. Results for the Maximal Elevations of Isotherms (ζ_m), Amplitudes of Velocity Components (u_m, v_m, w_m) and the Minimum of the Ray Slope $|R_{\min}|$ in Each Case of Figure 3

Case	ζ_m, m	u_m, cms^{-1}	v_m, cms^{-1}	w_m, cms^{-1}	$\lvert R_{\min}\rvert$
A	3.04	5.45	5.47	4.27×10^{-2}	7.8×10^{-3}
B	3.03	5.51	5.53	4.26×10^{-2}	7.71×10^{-3}
C	2.73	6.24	6.26	3.84×10^{-2}	6.13×10^{-3}
D	3.17	4.54	4.54	4.45×10^{-2}	9.8×10^{-3}
E	1.9	2.07	2.07	2.67×10^{-2}	1.29×10^{-2}

Haren and Millot [2004]). The corresponding limits of the ray slope R can be expressed as:

$$\lim R_1 = \frac{1-\Omega^{*2}\sin^2\theta}{\operatorname{sgn}(1-\Omega^{*2}\sin^2\theta)\cdot\sqrt{\Omega^{*2}-1}\,\frac{1}{2}\Omega^{*2}\sin 2\theta},$$
$$\lim R_2 = -\frac{1-\Omega^{*2}\sin^2\theta}{\operatorname{sgn}(1-\Omega^{*2}\sin^2\theta)\cdot\sqrt{\Omega^{*2}-1}+\frac{1}{2}\Omega^{*2}\sin 2\theta} \quad (21)$$

For superinertial waves ($\theta < \theta_c$), $\lim R_1$ denotes the upper limit of the right branch of the rays, and $\lim R_2$ the lower limit of the left branch. Conversely, for subinertial waves ($\theta > \theta_c$), $\lim R_1$ and $\lim R_2$ represent, respectively, the lower limit of the right branch and the upper limit of the left branch of the rays.

[21] To more closely diagnose the nontraditional effects, the dependence of the limits of ray angles, ν_m, on latitude θ are graphed in Figure 5, from which we can find, i.e., at $\theta = 15°$, the maximum ν of the right branch and minimum ν of the left branch of the rays are approximately 90° and 120°, respectively. This implies that at latitude $\theta = 15°$ the ray angle of the right branch is always below 90°, while that of the left branch is situated in the range from 120° to 180°.

[22] In particular, it is noteworthy that for the subinertial wave, the ray angle of the right branch meets a maximum, ν_m, as μ_0 equals zero, and at the same time, the two characteristic lines of internal waves are incorporated. The corresponding upper limit of the dimensionless frequency, N^*_m, when $\mu_0 = 0$, is:

$$N_m^{*2} = \frac{\Omega^{*2}-1}{\Omega^{*2}\sin^2\theta - 1} \quad (22)$$

As is obvious from Figure 2c, ray angles of the two branches become identical when the dimensionless frequency variable N^* reaches the upper limit N^*_m. The ray slope for this case is easily determined from equation (19) as:

$$R_m|_{N^*\to N^*_m} = 2\frac{\Omega^{*2}\sin^2\theta - 1}{\Omega^{*2}\sin 2\theta} = \frac{\sqrt{\Omega^{*2}-1}}{\sqrt{(N_m^{*2}-1)(N_m^{*2}+\Omega^{*2}-1)}} \quad (23)$$

The corresponding ray angles are represented by symbol cross as plotted in Figure 5, where the limiting value of the ray angles is specified, i.e., at latitude $\theta = 80°$ the approximate upper limit of the right branch or lower limit of the left branch is 30°. Note that along with the proximity of $N^* \to N^*_m$, the horizontal wavelength of the internal wave becomes infinitely long and the wave amplitude tends to zero.

4. Tidal Conversion

[23] For purposes of studying the internal tide generation and understanding the deep-ocean mixing, the most important issue is to estimate the rate at which energy is extracted from barotropic tide, and radiated into internal gravity waves at topographic features. In this paper the conversion rate is calculated following *Bell* [1975] and *Khatiwala* [2003]. The pressure field associated with the internal wave solutions derived previously exerts a net force on the bottom topography, which implies that net work is done by the background flow in generating the internal wavefield. The rate of work is the power, or the energy flux, P. In order to compute it an expression for pressure p is required. Eliminating u and v from the momentum equations gives:

$$\rho_0\left[(\partial_{tt}+f^2)\partial_z + ff_h\partial_y\right]w = p_{yyt} \quad (24)$$

Application of the Laplace and Fourier transforms results in:

$$(s^2+f^2)\tilde{\tilde{w}}_z + ikff_h\tilde{\tilde{w}} = -k^2 s\frac{\tilde{\tilde{p}}}{\rho_0} \quad (25)$$

Figure 3. (a) Density plots of the buoyancy field computed from equations (10) or (11) for a Gaussian profile. Parameters for the tide and topography are the same as those in Figure 1. The propagation is in the meridional direction. The latitude and nondimensional buoyancy frequency are $\theta = 74°$, $N^* = 0.2$. The maximal elevations of isotherms are found to be 3.04 m. (b) Density plots of the buoyancy field computed from equations (10) or (11) for a Gaussian profile. Parameters for the tide and topography are the same as those in Figure 1. The propagation is in the meridional direction. The latitude and nondimensional buoyancy frequency are $\theta = 74°$, $N^* = 0.958$. The maximal elevations of isotherms are found to be 3.03 m. (c) Density plots of the buoyancy field computed from equations (10) or (11) for a Gaussian profile. Parameters for the tide and topography are the same as those in Figure 1. The propagation is in the meridional direction. The latitude and nondimensional buoyancy frequency are $\theta = 74°$, $N^* = 5$. The maximal elevations of isotherms are found to be 2.73 m. (d) Density plots of the buoyancy field computed from equations (10) or (11) for a Gaussian profile. Parameters for the tide and topography are the same as those in Figure 1. The propagation is in the meridional direction. The latitude and nondimensional buoyancy frequency are $\theta = 75°$, $N^* = 0.963$. The maximal elevations of isotherms are found to be 3.17 m. (e) Density plots of the buoyancy field computed from equations (10) or (11) for a Gaussian profile. Parameters for the tide and topography are the same as those in Figure 1. The propagation is in the meridional direction. The latitude and nondimensional buoyancy frequency are $\theta = 75°$, $N^* = 3.3$. The maximal elevations of isotherms are found to be 1.9 m.

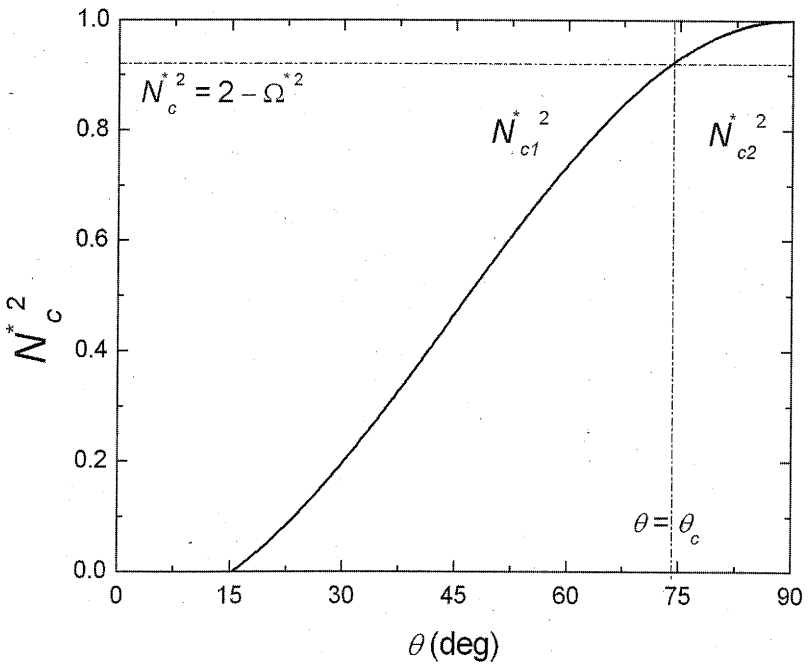

Figure 4. Critical value of dimensionless frequency N^* as a function of the latitude θ.

Substituting equation (9) into the above equation gives:

$$\tilde{\bar{p}}(k,-h_0) = i\rho_0 U_0 \frac{s^2+f^2}{s-i\omega_0}\frac{K\cot Kh_0}{ks}e^{st}\overline{H}(k) \tag{26}$$

After applying the inverse Laplace transform to the above equation, we obtain the following description for the Fourier transformation of p:

$$\bar{p}(k) = \frac{i\rho_0 U_0 \overline{H}(k)}{kh_0^2}\sum_{m=1}^{\infty}\frac{m\pi}{\omega_{1m}}\frac{\omega_{1m}^2 - f^2}{(\partial K/\partial s)_{s=i\omega_{1m}}} \cdot \left(\frac{e^{i\omega_{1m}t}}{\omega_{1m}-\omega_0} - \frac{e^{-i\omega_{1m}t}}{\omega_{1m}+\omega_0}\right) - \rho_0 U \frac{\omega_0^2 - f^2}{\omega_0}\frac{\overline{H}(k)}{k}K_1 \cdot \cot K_1 h_0 \tag{27}$$

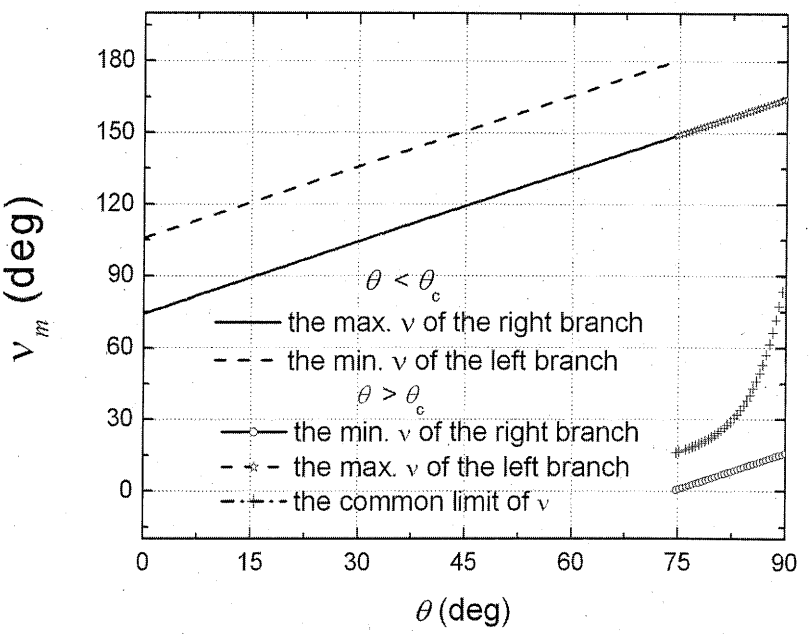

Figure 5. Limits of ray angles ν as a function of latitude θ. For superinertial waves, solid line corresponds to the upper limit of ν of the right branch, and dashed line to the lower limit of ν of the left branch. For subinertial waves, solid line plus symbol circle correspond to the lower limit of ν of the right branch), dashed line plus symbol star to the upper limit of ν of the left branch, and symbol cross to the common limit of ν of the two branches.

where

$$K_1(k) = \sqrt{\frac{(N^2-\omega_0^2)(\omega_0^2-f^2)+\omega_0^2 f_1^2}{(\omega_0^2-f^2)^2}}|k|, \tag{28}$$

Invoking the two-function version of Parseval's theorem, the work per unit cross-stream length acting on the topography can then be written as:

$$W(t) = \int_{-\infty}^{\infty} p(y,-h_0,t)\frac{dH}{dy}Udy = -i\int_{-\infty}^{\infty}\overline{p}(k,-h_0,t)k^*\overline{H}^*Udk \tag{29}$$

where * denotes complex conjugate. After substituting equation (27) into equation (29), the work is eventually given by:

$$W = 2\pi^2\frac{\rho_0 U^2}{h_0^2}\frac{|\omega_0^2-f^2|}{\omega_0\sqrt{\mu^2(i\omega_0)}}\sum_{m=1}^{\infty} m\left|\overline{H}(k_m)\right|^2 \tag{30}$$

Averaged over the fundamental period $2\pi/\omega_0$, the power per unit cross-stream length in the internal wavefield (vertical energy flux C) is expressed as:

$$C = \frac{\omega_0}{2\pi}\int_0^{2\pi/\omega_0} Wdt = \pi\frac{\rho_0 U_0^2}{h_0}\frac{|\omega_0^2-f^2|}{\omega_0}\sum_{m=1}^{\infty} k_m\left|\overline{H}(k_m)\right|^2 \tag{31}$$

For comparison with the traditional result, the result of *Khatiwala* [2003] for the tidal conversion is used, which is given as:

$$C_K = 4\rho_0\sum_{m=1}^{\infty}\sum_{n=1}^{n_0} J_n^2\left(\frac{k'_m U_0}{\omega_0}\right)\frac{n\omega_0}{m}\sqrt{(N^2-n^2\omega_0^2)(n^2\omega_0^2-f^2)}\cdot\left|\overline{H}(k'_m)\right|^2 \tag{32}$$

where

$$k'_m = \frac{m\pi}{h_0}\Big/\sqrt{\frac{N^2-\omega_0^2}{\omega_0^2-f^2}} \tag{33}$$

Invoking the relation of Bessel function for small y, $J_n(y) \approx (y/2)^n/n$, one can have that for small excursion parameter, kU_0/ω_0, the term for $n = 1$, the lowest harmonic, dominates in equation (32) [*St. Laurent and Garrett*, 2002; *Garrett and Kunze*, 2007], and Khatiwala's result hence reduces to:

$$C_K = \pi\frac{\rho_0 U_0^2}{h_0}\frac{\omega_0^2-f^2}{\omega_0}\sum_{m=1}^{\infty} k'_m\left|\overline{H}(k'_m)^2\right| \tag{34}$$

Thus it is apparent that if the traditional approximation, namely, $f_h = 0$, is adopted, the result of this paper C agrees well with Khatiwala's result C_K. Furthermore, it is straightforward to normalize the energy flux by a reference value, $C_0 = \rho_0 U_0^2\omega_0 H_0^2$, and the dimensionless conversion rates for a Gaussian topography, defined by $H(y) = H_0\exp(-y^2/2L^2)$, as:

$$\mathrm{X} = \frac{C}{C_0} = \pi\left|1-\Omega^{*2}\sin^2\theta\right|\gamma\sum_{m=1}^{\infty}\kappa_m e^{-\kappa_m^2} \tag{35}$$

and

$$\mathrm{X}_K = \frac{C_K}{C_0} = \pi\left(1-\Omega^{*2}\sin^2\theta\right)\gamma\sum_{m=1}^{\infty}\kappa'_m e^{-\kappa'^2_m} \tag{36}$$

where

$$\kappa_m = k_m L = m\pi\gamma\Big/\sqrt{\frac{(N^{*2}-1)(1-\Omega^{*2}\sin^2\theta)+\Omega^{*2}\cos^2\theta}{(1-\Omega^{*2}\sin^2\theta)^2}},$$
$$\kappa'_m = k'_m L = m\pi\gamma\Big/\sqrt{\frac{N^{*2}-1}{1-\Omega^{*2}\sin^2\theta}} \tag{37}$$

The nondimensional variables γ is defined as $\gamma = L/h_0$.

[24] The behavior of the conversion rate X as a function of the latitude θ is illustrated in Figure 6, and compared with X_K under the traditional approximation. As distinct from Figure 6 (*a*) where $N^* = 10$, the differences between X and X_K are indiscernible, implying the nontraditional effects are trivial for sufficiently large values of N^*. Furthermore, the curves with different values of γ show dissimilar performances against latitude θ. For $\gamma = 5$, tidal conversions are more powerful at lower latitudes and are a maximum near $\theta = 40°$, but, however, diminish rapidly for higher latitudes and approach zero when the latitude tends to the critical value. By contrast, for a wider topography ($\gamma = 10$), the tidal conversions are extremely weak at lower latitudes, and significant contributions occur principally at middle and higher latitudes ($50° < \theta < 70°$). This fact reveals a resonance character of internal tide generation over the ridge. Since latitude θ is connected with the horizontal wave number of the internal tide for a given N^*, Ω^* and the total depth h_0, as implied by equation (6), one can consequently recognize from equations (35) and (36) that the expressions of tidal conversion reflect a combined effect of two horizontal characteristic scales, i.e., the horizontal wave numbers of internal tide and the topography. It is difficult to determine directly from equations (35) and (36) how these two scales are affected and the location of the critical point is where the final effect is maximum, mostly due to the horizontal scale of the internal tide-a result by superimposition of infinite discrete waves of various wave numbers and amplitudes. Therefore the information can only be sought numerically and has been illustrated in Figure 6a, that is, the resonance latitudes where the conversions get the maximum are approximately 40°and 65° for $\gamma = 5$ and 10, respectively. This conclusion resembles that made by *Vlasenko et al.* [2003] who found amplitudes of the generated internal semidiurnal waves got their highest values upon different resonant latitudes for various values of the length of the underwater ridge. Another common feature in Figure 6a is that the two curves both end at the critical latitude, indicating that above the critical latitude the

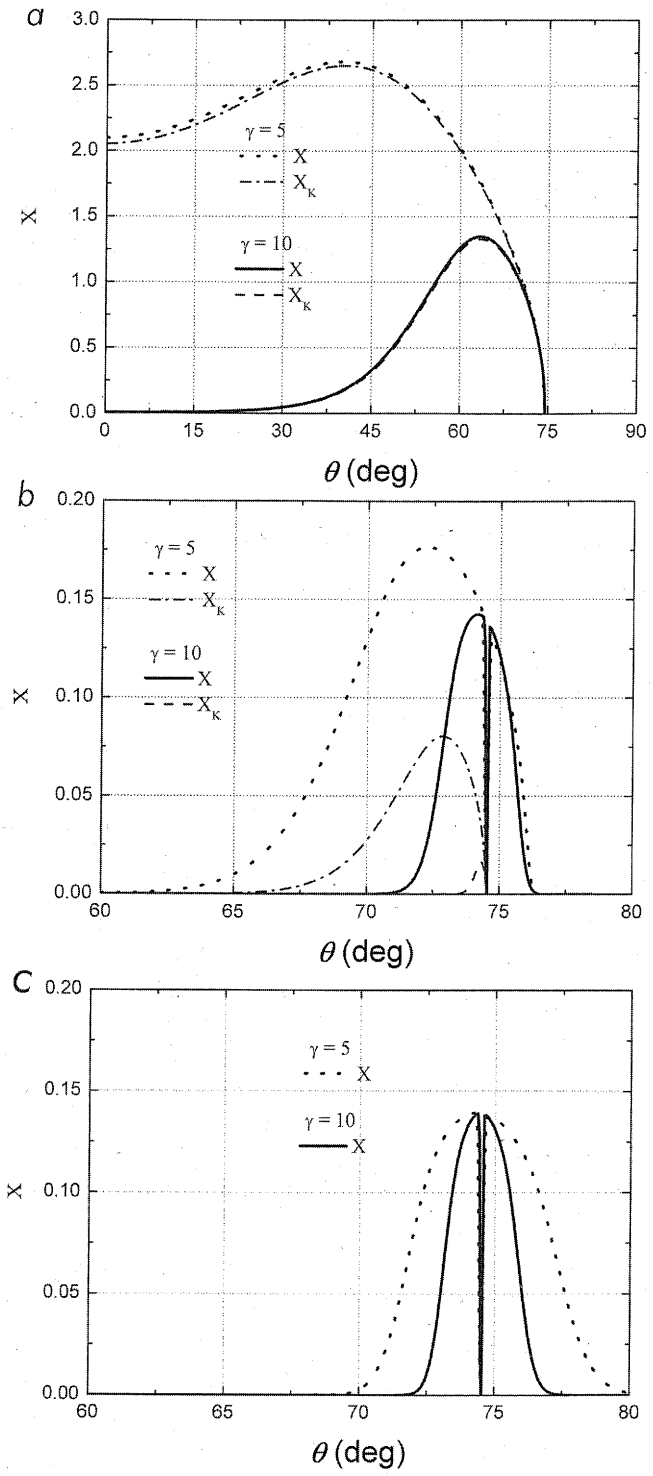

Figure 6. (a) Behavior of X as a function of θ ($N^* = 10$). (b) Behavior of X as a function of θ ($N^* = 1.5$). (c) Behavior of X as a function of θ. ($N^* = 0.5$).

internal tide cannot be generated in oceans with strong stratifications.

[25] In Figure 6b the nondimensional buoyancy frequency drops to 1.5 and at this stage the difference between the conversion rates X and X_K becomes remarkable. At subcritical latitudes, an increase of γ decreases the conversion rate, but increases the difference between X and X_K. Also, it can be noted that the resonant latitude increases with γ. Above the critical latitude, the effect of γ is insignificant. The most important conclusion is that the conversion rate made without invoking the traditional approximation is notably higher than that under this approximation. This finding indicates that effects due to the account of horizontal component of the Earth's rotation become significant, or, in other words, the traditional approximation turns to be quite inapplicable, as the buoyancy frequency is close to that of the tide. It should be noted that oceans with such a characteristic stratification are possibly quite rare, although that has not been established yet. Thus it would be helpful if the probability of such situations can be estimated using available data. However, this task is not the major objective of this study and is planned for a future study.

[26] For $N^* = 0.5$ as depicted in Figure 6c, the tidal conversion under the traditional approximation is zero, implying that internal tide cannot be generated under this approximation neither for supercritical nor subcritical latitudes. However, if the horizontal component of the Coriolis vector is accounted for, there is still considerable energy converted from the barotropic tide to the internal tide. This is the most important conclusion of this paper. The effect of the horizontal scale of the topography is also evident. The conversion rate is confined in a narrow range from the critical latitude. Increasing γ decreases the range, but the maximum value of the conversion rate keeps almost unchanged. Generally, the major conclusion of this part is that the internal tide can be generated freely beyond the critical latitude in a weakly stratified ocean, which provides another substantial explanation for the observations by *Pisarev* [1996] and *Parsons et al.* [1996] besides that made by *Vlasenko et al.* [2003] accounting mainly for the occurrence of nonlinear waves.

5. Conclusions

[27] The objective of this paper is motivated by a contradiction that above the critical latitude the existing linear theories of baroclinic tides prohibit the tidal activity, while in situ data have revealed evidence of semidiurnal internal tides. For the purpose of studying the physical mechanisms of the generation of internal tides at high latitudes and understanding the basic parameters that control their excitation, a linear model is constructed, taking both the vertical and horizontal components of the Earth's rotation into consideration. Analytical solutions for the generation of internal tides have been derived with the aid of transient wave method, providing an important conclusion that the wave properties differ fundamentally from those under the "traditional approximation" on the *f*-plane.

[28] The most pronounced change in the attributes of internal waves due to the presence of nontraditional terms is the asymmetry of internal wave ray paths. For various combinations of latitude θ and dimensionless buoyancy frequency N^*, propagating directions of rays can basically have five kinds of modes: (1) both equatorward, (2) both poleward, (3) equatorward plus vertical, (4) poleward plus vertical, and (5) poleward plus equatorward. The findings of the modes, both equatorward and both poleward, agree with

Durran and Bretherton [2004] and *Gerkema and Shrira* [2005b]. Furthermore, under the traditional approximation the singular limit of the ray slope develops at which the rays propagate vertically as the critical condition $N^* = 1$ is approached. However, this tidal limit at $N^* = 1$ is healed and two other kinds of critical conditions for the ray angle being 90° are created by nontraditional effects, which are $N^{*2}_c = 1 - \Omega^{*2} \cos^2\theta$ and $\theta = \theta_c$. The former condition ensures that the right branch or the left branch favors the vertical direction, depending on whether latitude θ is below or above the critical latitude θ_c. On the other hand, the latter critical condition permits the right branch to propagate vertically at the critical latitude, perpendicular to the left branch.

[29] The conversion rate for a Gaussian topography is calculated and compared with the result made under the traditional approximation. For a sufficiently large value of N^*, the two results are approximately identical, and both end at the critical latitude, indicating that above the critical latitude the internal tide cannot be generated in oceans with strong stratifications. A resonance characteristic of internal tide generation created by the interplay between the internal wave and the topography is revealed. A wider topography corresponds to a higher resonant latitude where the conversion rate reaches the maximum. If the buoyancy frequency is close to the tidal one the differences between the two kinds of conversion rates become remarkable. The conversion rates made without invoking the traditional approximation show notably higher than those under this approximation. This finding indicates that the traditional approximation turns out to be quite irrelevant in such a situation. For a weakly stratified ocean (N^* less than 1), the traditional approximation leads to that no energy can be converted from the barotropic tide to the internal tide. In other words, under this approximation the internal tide cannot be generated either for supercritical or subcritical latitudes. However, if the horizontal component of the Coriolis vector is considered, a substantial conversion can still occur in the weakly stratified ocean, although which may be quite rare but still possible.

[30] **Acknowledgments.** This work was supported by the National Natural Science Foundation of China under grant 10602060.

References

Baines, P. G., and J. W. Miles (2000), On topographic coupling of surface and internal tides, *Deep Sea Res., Part I, 47*, 2395–2403.

Bell, T. H. (1975), Lee waves in stratified flows with simple harmonic time dependence, *J. Fluid Mech., 67*, 705–722.

Durran, D. R., and C. Bretherton (2004), Comments on "The roles of the horizontal component of the earth's angular velocity in non-hydrostatic linear models", *J. Atmos. Sci., 61*, 1982–1986.

Eckart, C. (1960), *Hydrodynamics of Oceans and Atmospheres*, Elsevier, New York.

Garrett, C., and E. Kunze (2007), Internal tide generation in the deep ocean, *Annu. Rev. Fluid Mech., 39*, 57–87.

Gerkema, T., and V. I. Shrira (2005a), Near-inertial waves on the "nontraditional" β plane, *J. Geophys. Res., 110*, C01003, doi:10.1029/2004JC002519.

Gerkema, T., and V. I. Shrira (2005b), Near-inertia waves in the ocean: Beyond the "traditional approximation", *J. Fluid Mech., 529*, 195–219.

Hendershott, M. C. (1981), Long waves and ocean tides, in *Evolution of Physical Oceanography*, edited by B. A. Warren and C. Wunsch, pp. 292–341, MIT Press, Cambridge, Mass.

Khatiwala, S. (2003), Generation of internal tides in an ocean of finite depth: Analytical and numerical calculations, *Deep Sea Res., Part I, 50*, 3–21.

LeBlond, P. H., and L. A. Mysak (1978), *Waves in the Ocean*, Elsevier, New York.

Lighthill, J. (1978), *Waves in Fluid*, Cambridge Univ. Press, New York.

Miropol'sky, Yu. Z. (2001), *Dynamics of Internal Gravity Waves in the Ocean*, Kluwer, Academic Publishers, London.

Nayfeh, A. H. (1973), *Perturbation Methods*, Wiley, New York.

Parsons, A. R., R. H. Bourke, R. D. Muench, C. S. Chiu, J. F. Lynch, J. Miller, H. A. J. Plueddemann, and R. Pawlowicz (1996), The Barents Sea Polar Front in summer, *J. Geophys. Res., 101*(C6), 14,201–14,221.

Pisarev, S. V. (1996), Low-frequency internal waves near the shelf edge of the Arctic basin, *Oceanology, 36*(6), 771–779.

Saint-Guily, B. (1970), On internal waves. Effects of the horizontal component of the earth's rotation and of a uniform current, *Deutsche Hydrograph. Z., 23*, 16–23.

St. Laurent, L., and C. Garrett (2002), The role of internal tides in mixing the deep ocean, *J. Phys. Oceanogr., 32*, 2882–2899.

Van Haren, H. (2006), Asymmetric vertical internal wave propagation, *Geophys. Res. Lett., 32*, L24614, doi:10.1029/2005GL023915.

Van Haren, H., and C. Millot (2004), Rectilinear and circular inertial motions in the western Mediterranean Sea, *Deep Sea Res., Part I, 51*, 1441–1455.

Van Haren, H., and C. Millot (2005), Gyroscopic waves in the Mediterranean Sea, *Geophys. Res. Lett., 32*, L24614, doi:10.1029/2005GL023915.

Vlasenko, V., N. Stashchuk, K. Huntter, and K. Sabinin (2003), Nonlinear internal waves forced by tides near the critical latitude, *Deep Sea Res., Part I, 50*, 317–338.

P. Fan, Institute of Mechanics, Chinese Academy of Sciences, No. 15 Beisihuanxi Road, Beijing (100190) China. (fanping@imech.ac.cn)

V. P. Singh, Department of Biological and Agricultural Engineering, Texas A & M University, Scoates Hall, 2117 TAMU, College Station, TX 77843-2117, USA. (vsingh@tamu.edu)